Int. J. Electrochem. Sci., 13 **(2018)** 3997 – 4025, doi: 10.20964/2018.04.59

International Journal of ELECTROCHEMICAL SCIENCE
www.electrochemsci.org

The inhibition Activity of 1,10 - bis(2-formylphenyl)-1,4,7,10-tetraoxadecane (Ald) and its Schiff base (L) on the Corrosion of Carbon Steel in HCl: Experimental and Theoretical Studies

Lamia Boucherit[1,*], *Tahar Douadi*[1], *Nadjib Chafai*[1], *Mousa Al-Noaimi*[2], *Salah Chafaa*[1]

[1] Laboratoire d'électrochimie des matériaux moléculaires et complexes (LEMMC), Département de Génie des Procèdes, Faculté de Technologie, Université Ferhat ABBAS de Sétif-1, 19000 Sétif, Algeria
[2] Department of Chemistry, Hashemite University, P.O. Box 150459, Zarqa 13115, Jordan
[*]E-mail: boucheritlm49@gmail.com

Received: 31 December 2017 / *Accepted:* 7 February 2018 / *Published:* 6 March 2018

The inhibitor effect of aldehyde and their Schiff base ligand on the corrosion of XC48 carbon steel in 1M HCl solution was investigated using weight loss measurements and electrochemical Methods. These compounds are an efficient corrosion inhibitors and their inhibition efficiency are increased with increasing inhibitor concentration. The Adsorption of these compounds on carbon steel surface obeys Langmuir's isotherm. The surfaces of carbon steel after exposing to test solutions were examined by atomic force microscopy. The quantum chemical parameters were calculated using the density functional method. The interaction between the Fe(100) surface and the inhibitors were performed by molecular dynamics simulations.

Keywords: Schiff base, DFT, MDS, AFM, Corrosion inhibition.

1. INTRODUCTION

The use of corrosion inhibitor is one of the most effective measures for protecting metal surfaces against corrosion in acid environments. Some organic compounds are found to be effective corrosion inhibitors for many metals and alloys [1-3]. Generally, inhibitor molecules may physically or chemically adsorb on a metal surface forming an adsorption layer that functions as a barrier protecting the metal from the corrosion [4-6].

Acid solutions are widely used to remove unwanted sediments and rust in many industrial processes [7-8]. Adsorption depends on the charge of the metal but on the chemical structure of the inhibitor [9-10]. The efficiency of Schiff's bases is much higher than that of corresponding aldehyde

and amines due to the presence of a -C=N- group in the molecules [11-12]. The planarity and lone pairs of electrons on N atoms are important for the adsorption of Schiff's base molecules on a metal surface. Also, Organic compounds containing heteroatoms such as N, O and S have been reported as being efficient corrosion inhibitors for metals and alloys [13-16].

The aim of the present work is to investigate the inhibitory action of aldehyde and there Schiff base, named 1,10 - bis(2-formylphenyl)-1,4,7,10- tetraoxadecane *(***Ald***)* and 1,18-diaza-(3,4;15,16;-dibenzo)-19,27-oxydianiline-5,8,11,14-tetra oxa cycloheptacosine-1,17-diene ***(L).***

The research was done on carbon steel in HCl aggressive medium at different temperatures and different immersion times by electrochemical methods and weight loss. The effect of concentrations of HCl on the inhibition efficiencies was also studied. Morphological changes on the corroding steel surface have been visualized by atomic force microscopy (AFM).

In this study, the thermodynamic and kinetic parameters for carbon steel XC48 corrosion and the inhibitive properties of (**L**) and (**Ald**) were determined. The experimental results were associated with a theoretical method and discussed.

2. EXPERIMENTAL

2.1. Inhibitors

The studied (**L**) Schiff base and Aldehyde (**Ald**) were synthesized in proper literature [17].

The molecular structures of inhibitors are shown in Fig.1.

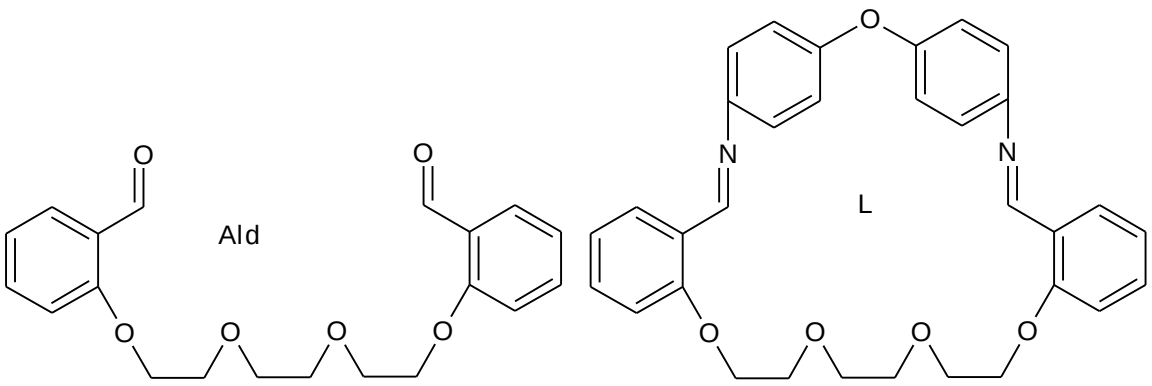

Figure 1. The structures of the investigated compounds (L) and (Ald).

2.2. Materials

XC48 carbon steel specimens are used for all corrosion tests. Their chemical composition is (wt.%) : C = 0,418%, Mn = 0,730%, Mo = 0,012%, P = 0,016%, S = 0,019 %, Si = 0,245% Ni = 0,079%, F = 0,777% and Fe = 98.0.9873%. The surfaces of the XC48 working electrodes were successively cleaned with SiC abrasive papers (600, 800, 1000, 1200 and 1800 grades), washed with distilled water and degreased with acetone and finally dried at room temperature.

2.3. Solutions

The corrosive solution, 1 M HCl, 2M HCl were prepared by dilution of analytical grade 37% HCl of predetermined normality with double distilled water. The concentration (C_{RW}) of the inhibitors is within this range 10^{-5}–10^{-3} M.

2.4. Weight loss measurements

Gravimetric experiments were carried out in glass vessel containing 40 ml of the corrosive test solution for 24 h at 25 C°.

The inhibition efficiency of the inhibitor was calculated Eq.1

$$EI_W\% = \left(1 - \frac{W'_{corr}}{W_{corr}}\right) \times 100 \quad \text{..... (1)}$$

$$W_{corr} = \frac{\Delta m}{tS}$$

$$\Delta m = m_1 - m_2$$

$$\theta = \left(1 - \frac{W'_{corr}}{W_{corr}}\right) \quad \text{.....(2)}$$

Where W_{corr} and W'_{corr} are corrosion rates in (mg. cm^{-2}. h^{-1}), which are related to the values of the weight loss of steel after immersion in solutions without and with inhibitor, respectively and is (θ) the surface coverage.

2.5. Electrochemical measurements

The electrochemical measurements were carried using a PGZ 301 voltlab 40 and Voltamaster 4 software. All the electrochemical studies were carried out in a conventional three electrode set up, open to atmosphere. a XC48 carbon steel as the working electrode (WE) and a Carbon as the counter electrode (CE), a saturated calomel electrode (SCE) as the reference electrode (RE).

The working electrode was first immersed into the test solution for 30 min to establish a steady state open circuit potential (OCP), then the polarization curves in the range of −800 to −200 mV was obtained using a 0.5 mV/s scan rate. The corrosion rates were obtained from the polarization curves by linear extrapolation of the anodic and cathodic arms of the Tafel plots as well as the corrosion potential (E_{corr}).

We used The following equation to calculate the inhibition efficiency obtained from the polarization curves $EI_p(\%)$

$$EI_p(\%) = \left(\frac{i_{corr} - i_{corr(inh)}}{i_{corr}}\right) x100 \quad \text{..... (3)}$$

where i_{corr} and $i_{corr(inh)}$ represents the corrosion current density values in the absence and presence of inhibitor respectively. The values of the surface coverage (θ) were calculated using the following equation

$$\theta = \frac{i_{corr} - i_{corr(inh)}}{i_{corr}} \quad \text{..... (4)}$$

Electrochemical impedance (EIS) measurements were performed at open circuit potential (OCP) with 100 kHz to 10 mHz frequency range, with a 10 mV signal amplitude perturbation then Nyquist plots were drawn from these experiments.

The Inhibition efficiency obtained from the electrochemical impedance spectroscopy ($EI_{SIE}(\%)$) was calculated by the following equation

$$EI_{SIE}(\%) = \frac{R\,t(inh) - R\,t(0)}{R\,t(inh)} x100 \quad \text{.....(5)}$$

where $R_{t(0)}$ and $R_{t(inh)}$ are respectively the values of the charge transfer resistances of steel before and after addition of inhibitor.

2.6. Measurement of the potential of zero charge

We studied using impedance measurements, the influence of the load of the steel electrode on the capacity of the double layer by applying different potentials. The values of double layer capacitance (Cdl) were plotted against the potentials to determine the PZC after carbon steel immersed in 1 M HCl solutions containing 10^{-3}M of inhibitors.

2.7. Adsorption isotherm

To understand the interaction between the metal surface and the inhibitor Freundlich, Temkin and Langmuir isotherms of using surface coverage (θ) values of different concentrations of inhibitors (**L**) and (**Ald**) were obtained from measurements of potentiodynamic polarization.

2.8. Surface characterization (Atomic force microscopy)

The Atomic Force Microscopy AFM using an Asylum Research MFP-3D Classic AFM instrument was used to investigate The surface morphology of the polished carbon steel before and after 24 h of immersion in 1 M HCl without and with inhibitors, respectively.

3. COMPUTATIONAL DETAILS

3.1. Quantum chemical calculations

We used GAUSSIAN 09 W standard software [18] and GaussView 5.0.8 software for all quantum chemistry calculations [19], and the density function theory method (DFT / B3LYP) with a database of 6-31 G (d, p) in the gaseous phases [20, 21] for the optimization of the geometry of the synthesized compound.

Quantum chemical parameters such as global hardness (η), energy deviation ΔEGAP, absolute electronegativity (χ), overall softness (σ), electrophile index (ω) and fraction of electrons transferred (ΔN) are calculated using the following equations [22-24]:

$$\Delta E_{GAP} = E_{LUMO} - E_{HOMO} \quad (6)$$

$$\eta = \frac{E_{LUMO} - E_{HOMO}}{2} \quad (7)$$

$$\sigma = 1/\eta \quad (8)$$

$$\chi = \frac{-(E_{HOMO} + E_{LUMO})}{2} \quad (9)$$

$$\omega = \frac{\chi^2}{2\eta} \quad (10)$$

$$\Delta N = \frac{\chi_{Fe} - \chi_{inh}}{[2(\eta_{Fe} + \eta_{inh})]} \quad (11)$$

where $\boldsymbol{\chi_{Fe}}$ and $\boldsymbol{\chi_{inh}}$ Are the absolute electronegativity of metal and inhibitor molecules respectively. $\boldsymbol{\eta_{Fe}}$ and $\boldsymbol{\eta_{inh}}$ Are the absolute hardness of metal and the inhibitor molecule, respectively. The theoretical value of $\boldsymbol{\chi_{Fe}}$ is 7.0 eV and $\boldsymbol{\eta_{Fe}}$ is 0 for the computation of the fraction transferred electrons [25].

3.2. Molecular dynamic simulations

We performed dynamic molecular simulations using a commercial software package called Materials Studio 7.0 developed by Accelrys Inc [26]. Herein, three modules were employed: Forcite module where the molecular structure of the compounds synthesized in a gas and aqueous phases was geometrically fully optimized. to identify possible adsorption configurations we used Adsorption locator module. A simulation box of 17.20 × 22.93 × 22.93 ˚A dimensions module was used for molecular dynamic simulations of the interaction between the inhibitor molecule and Fe (100) surface. The periodic boundary conditions were used in all three directions and the equations of motion were integrated within the canonical ensemble NVT. The Fe slab, the water slab containing the studied inhibitor and a vacuum layer were included in the simulation box. We employed a temperature of 298 K controlled by the Nose method using the COMPASS force field.

4. RESULTS AND DISCUSSION

4.1. Weight loss measurement

The weight loss measurements are used to study the inhibition of the corrosion of a metal in an electrolytic solution [27]. This method has the advantage of being of simple and not to require significant equipment. Table 1 shows the weight loss experiments in the presence of different concentrations of (**L**) and (**Ald**).

It is clear that the rate of corrosion decreases and the inhibition efficiency (EI_w%) increases with the increasing concentration of the inhibitor and reaches the maximum at the concentration of 1×10^{-3}M. This behavior can be attributed to the increase in the adsorption of (**L**) and (**Ald**) at the metal / solution interface when EI_W% is equal to 94.82% and 91.89%, for (**L**) and (**Ald**),

respectively. The increase in the inhibition efficiency with increasing concentration of inhibitors can be explained by increase of the surface coverage which delayed the dissolution of the metal [28].

Table 1. Weight loss results of mild steel corrosion in 1M HCl with addition of various concentrations of **L** and **Ald** at 25 °C.

Inhibitor	*C* (M)	*W*(mg/cm^2.h)	EI_w (%)
	0	2.7777	-
L	$1x10^{-5}$	0.4121	85.16
	$5x10^{-5}$	0.2997	89.21
	$1x10^{-4}$	0.1905	93.14
	$5x10^{-4}$	0.1519	94.53
	$1x10^{-3}$	0.1438	94.82
Ald	$1x10^{-5}$	0.3436	87.63
	$5x\ 10^{-5}$	0.3308	88.09
	$1x10^{-4}$	0.2680	90.35
	$5x10^{-4}$	0.2455	91.16
	$1x10^{-3}$	0.2252	91.89

4.2. Impedance Measurements

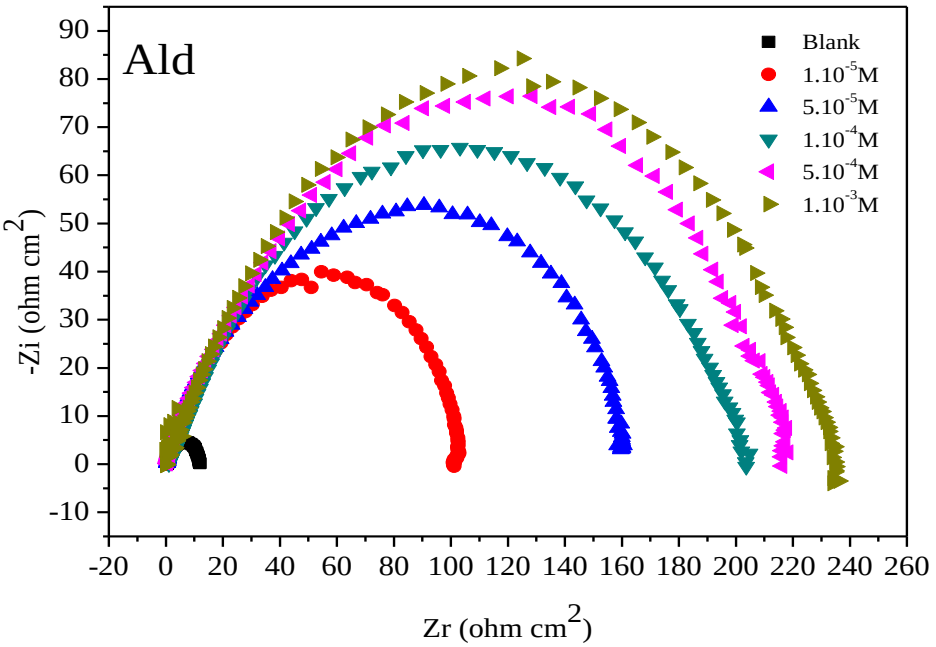

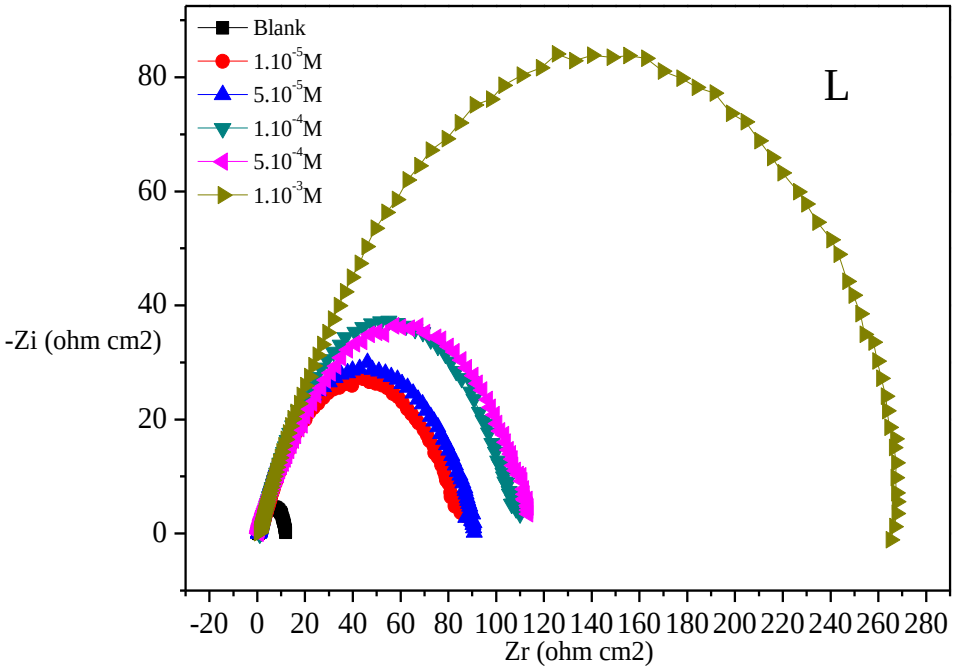

Figure 2. Nyquist impedance diagrams for carbon steel obtained at 25 °C in 1 M HCl solution containing different concentrations of title compounds.

Table 2. SIE parameters for the corrosion of mild steel in 1M HCl solution without and with different concentrations of **L** and **Ald** at 25 ℃.

Inhibitor	C (M)	R_s (Ω cm^2)	R_{ct} (Ω cm^2)	C_{dl} (μF cm^{-2})	EI_{SIE}(%)
	0	0.608	12.06	659.7	-
L	1×10^{-5}	1.594	84.72	525.9	85.76
	5×10^{-5}	0.718	90.22	441.0	86.63
	1×10^{-4}	1.515	107.60	662.2	88.79
	5×10^{-4}	1.020	115.60	192.6	89.56
	1×10^{-3}	1.246	279.00	203.0	95.67
Ald	1×10^{-5}	0.638	107.50	186.4	88.78
	5×10^{-5}	0.655	163.80	48.57	92.63
	1×10^{-4}	1.794	202.20	280.0	94.03
	5×10^{-4}	1.415	218.20	91.90	94.47
	1×10^{-3}	1.196	232.90	136.6	94.82

The impedance spectra for mild steel in 1M HCl in the absence and presence of various concentrations of (**L**) and (**Ald**) is shown in Fig 2 and its data is listed in table 2. The impedance diagrams obtained consist of a single capacitive loop which is not a perfect semicircle, and this is

attributed to the dispersion of the frequency of the interfacial impedance due to the heterogeneity of the surface of the electrode [29,30]. This heterogeneity may result from roughness, impurities, and dislocations, adsorption of the inhibitor and formation of porous layers [31]. This type of diagram is generally interpreted as a mechanism of transfer of charges on a heterogeneous and irregular surface [32]. The diameter of the capacitive semicircles is increased by increasing the concentration of inhibitor. It is clear that the addition of the inhibitor increases the values of the charge transfer resistor R_{ct}. The inhibitory efficiency increases with increasing inhibitor concentration.

The representative equivalent electrical circuit (CPE) in the case of adsorption of the compounds (**L**) and (**Ald**) is represented in figure 3. This circuit consists of the electrolyte resistance (R_s), a constant phase element (CPE) positioned in parallel with a charge transfer resistor (R_{ct}) [33].

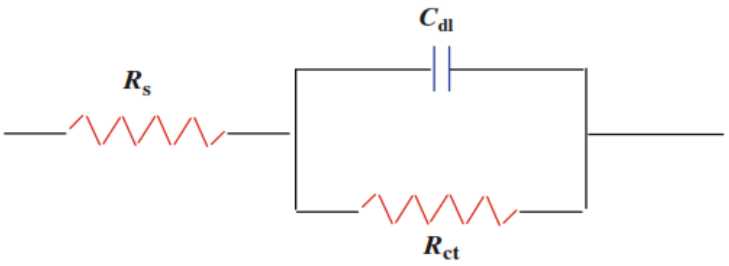

Figure 3. Electrical equivalent circuit used for modeling metal/solution interface in the absence and presence of inhibitors.

4.3. Potentiodynamic Polarization Studies

4.3.1. Effect of inhibitors concentration

Fig 4. Shows the representative Tafel polarization curves recorded on the carbon steel in 1M HCl in the absence and in the presence of different concentrations of (**L**) and (**Ald**) at 25 °C. In order to study the kinetics of the corrosion, certain electrochemical parameters such as corrosion potential (mV/cm^2), EIP inhibition efficiency (%), the corrosion potential E_{corr} (mV/SCE), the cathode and anode slopes of Tafel β_c and β_a are needed. It is noted that the values of i_{corr} decrease and that the PIE increases with the increase in inhibitor concentration. Also, there is an increase in the blocked fraction of the surface of the electrode by adsorption [34] through unbonded electron pairs of nitrogen and oxygen atoms as well as π-electrons [35]. The presence of the inhibitors in solution leads to the modification of both the cathodic and anodic polarization branches and slightly displaces the corrosion potential towards more negative potentials compared to the result obtained in the absence of inhibitor. This result indicates that the reduction of hydrogen is reduced by the addition of inhibitors and these compounds are mixed inhibitors [36].

The reduction of H^+ ions at the surface of mild steel is mainly due to a charge transfer mechanism because the Tafel cathode curves give rise to parallel lines with increasing inhibitor concentration and the addition of (**L**) or (**Ald**) does not alter the mechanism of evolution of hydrogen [37].

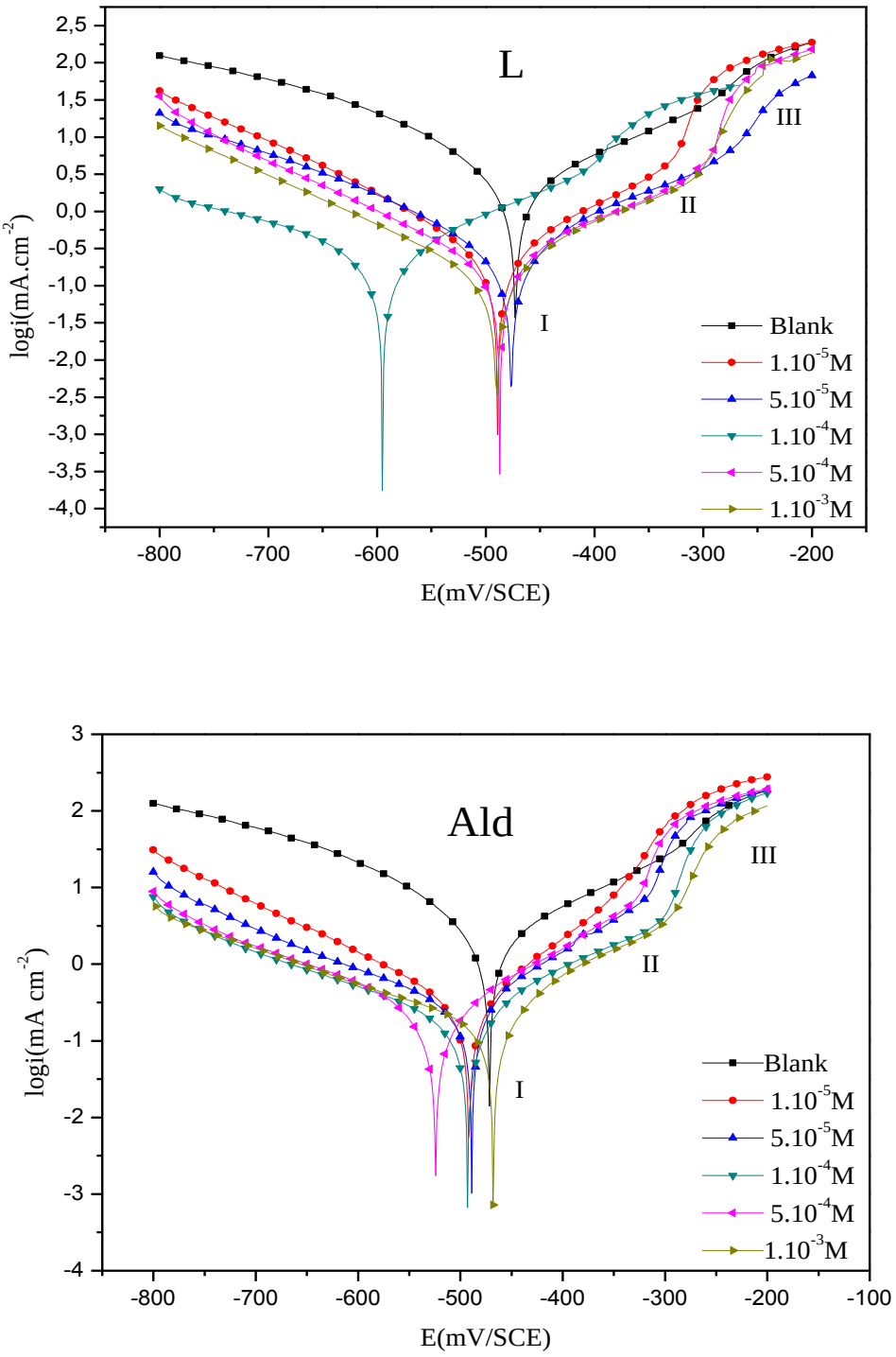

Figure 4. Tafel polarization curves for carbon steel obtained at 25 °C in 1 M HCl solution containing different concentrations of title compounds.

In anodic polarization curves, three parts for the inhibited region (I), flat region (II) and the uninhibited region (III) is shown in Figure 3. The increase of the anode potentials leads to an increase of the anode currents to a slope of ba1 in the region (I). And After exceeding a certain potential to region (II), the desorption potential (E_{des}) is found and a relative plane is observed at this stage. In this

case we have the equilibrium of the adsorption and desorption of the inhibitory molecules on the surface of the steel [38]. For region (III), there is a drastic change for anodic current densities, causing a large increase in the Tafel slope in the region of high polarization potentials. The large increase in the current is related to the marked desorption of the adsorbed inhibitor [39]. According to Solmaz [40, 41], the observation of the anodic curve is due to that the film which is made by inhibitor acts as a protective barrier on the surface of the steel. At this stage, dissolution of the metal lead to deformation of the inhibitor film on the metal surface and strongly increasing current in the Region (III) [42].

4.3.2. Effect of immersion time

The immersion time is a very important parameter in the evaluation of the stability of the corrosion inhibitors. In this way, a Tafel polarization is particularly useful technique for long time tests. Tafel polarization experiments were performed after different immersion times (0.5–120 h) at the optimal concentration of **(L)** and (**Ald**) (10^{-3}M) in 1 M HCl at 25°C. The values of corrosion current density (i_{corr}), corrosion potential (E_{corr}), cathodic and anodic Tafel slopes (βc and βa) at different immersion times at 25 ° C are summarized in the Table 3 .

Table 3. Influence of immersion time on electrochemical parameters of carbon steel electrode immersed in 1 M HCl at $1x10^{-3}$ M of **L** and **Ald.**

Inhibitor	*t* (h)	$-E_{corr}$ (mV/SCE)	$-\beta_c$ (mV/dec)	β_a (mV/dec)	I_{corr} (mA cm^{-2})	EI_p (%)	θ
Blank	0.5	471.9	77.3	85.5	1.2262	-	-
	24	508.0	82.4	134.4	1.4463	-	-
	48	495.4	62.6	87.2	1.4939	-	-
	72	497.1	81.6	131.6	2.0251	-	-
	96	497.1	82.0	131.0	2.0080	-	-
	120	497.0	82.4	127.2	2.1003	-	-
L	0.5	491.1	105.5	78.3	0.0810	93.39	0.93
	24	526.0	94.1	66.6	0.1100	92.39	0.92
	48	594.9	99.2	88.4	0.1163	92.21	0.92
	72	476.1	84.9	74.2	0.1220	93.97	0.93
	96	492.8	79.4	64.9	0.0926	95.38	0.95
	120	491.0	72.8	67.6	0.0241	98.85	0.98
Ald	0.5	467.8	129.8	71.8	0.0997	91.86	0.91
	24	515.8	78.0	67.9	0.1281	91.14	0.91
	48	555.9	75.4	96.9	0.3119	79.12	0.79
	72	506.3	79.6	98.3	0.4684	77.04	0.77
	96	548.1	84.6	105.7	1.0694	46.74	0.46
	120	495.6	81.7	130.6	1.8732	10.81	0.10

The excellent inhibition properties of (**L**) at 25 ° C can be obtained after 120 h of immersion in the acidic medium. Herein, and it can be suggested that the adsorption mechanism involves two types

of interactions: Chemisorption and physisorption. Alternatively, the (**Ald**) molecules form a compact film in a 24 hour, after this time they begin to be detached from the surface of the electrode causing the slow decrease in *E*Ip.

The inhibition efficiency is increased up to 98.85% when the immersion time is 120 hours for L , indicating a massive absorption rate on the surface of the carbon steel, The film reaches a more compact and uniform along with prolong immersion time

Also the inhibition efficiency decreases to 10.81% of Ald with the lengthening of time to 120 hours , The reasons can be attributed to the film torn from the inhibitor, which depends on the time of immersion

4.3.3. Effect of HCl concentration

It is clear from table 4 that the inhibition efficiency decreases with gradually increase of acid concentration from 1 to 2M indicates that the inhibitors are more effective at low concentration (1M). Fig 5 shows the effect of the aggressive media concentration on the polarization curves in absence and in presence of different concentrations of (**L**) and (**Ald**) at 25 °C. A uniform corrosion is since that the anodic polarization curves in presence of inhibitors break the anodic polarization curve in absence of inhibitors in a conman point E_b. On the other hand, this phenomenon is due to the formation of anodic protective films containing oxides, (**L**) and (**Ald**) [43, 44].

Table 4. Electrochemical parameters of carbon steel electrode immersed in 2 M HCl at different concentrations of **L** and **Ald** at 25°C .

Inhibitor	C (M)	$-E_{corr}$ (mV/SCE)	$-B_c$ (mV/dec)	B_a (mV/dec)	I_{corr} (mA cm^{-2})	EI_p (%)	θ
	0	539.1	62.7	73.2	1.3820	-	-
	1x10^{-5}	585.8	67.8	91.6	0.3205	76.80	0.76
	5x10^{-5}	595.9	78.0	101.5	0.2318	83.22	0.83
L	1x10^{-4}	574.1	73.3	88.4	0.2051	85.15	0.85
	5x10^{-4}	506.1	57.9	66.4	0.1962	85.80	0.85
	1x10^{-3}	574.1	109.9	79.3	0.1321	90.44	0.90
	5x10^{-5}	593.0	70.1	91.1	0.3981	71.19	0.71
	5x 10^{-5}	551.0	68.0	82.2	0.2941	78.71	0.78
Ald	1x10^{-4}	601.8	80.8	104.4	0.2533	81.67	0.81
	5x10^{-4}	600.9	82.1	109.0	0.2273	83.55	0.83
	1x10^{-3}	552.0	119.1	76.1	0.1621	88.27	0.88

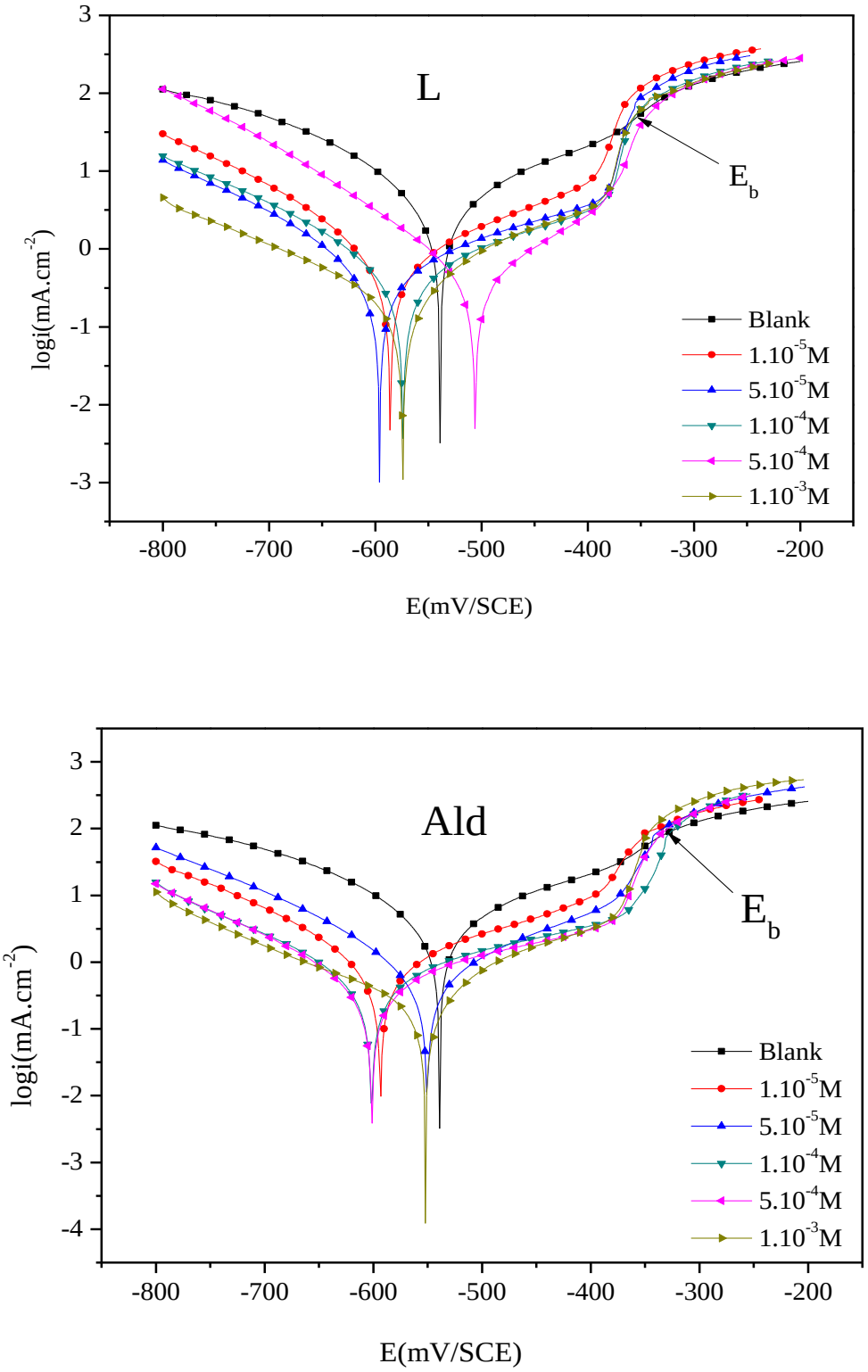

Figure 5. Tafel polarization curves for carbon steel obtained at 25 °C in 2 M HCl solution containing different concentrations of title compounds.

4.3.4. Effect of temperature

The effect of temperature on the inhibition efficiency for carbon steel in 1M HCl solution in the absence and the presence of different concentrations of inhibitors at a temperature ranging from 25 to 55 °C was studied. The obtained results are grouped in tables 5 and 6. It is found that the inhibitory efficiencies decrease with the increase of the temperature due to desorption of the inhibitors from the surface of the carbon steel.

Table 5. Influence of temperature on electrochemical parameters of mild steel electrode immersed in 1 M HCl at different concentrations of **L** .

T (°C)	C (M)	$-E_{corr}$ (mV/SCE)	$-B_c$ (mV/dec)	B_a (mV/dec)	i_{corr} (mA cm^{-2})	EI_p (%)	θ
	0	471.7	77.3	98.5	1.2262	-	-
	1x10^{-5}	489.1	79.2	72.7	0.1265	89.68	0.89
	5x10^{-5}	476.1	84.9	74.2	0.1220	90.05	0.90
	1x10^{-4}	594.9	99.2	88.4	0.1163	90.51	0.90
25	5x10^{-4}	487.2	91.3	77.0	0.0995	91.88	0.91
	1x10^{-3}	491.1	105.5	78.3	0.0810	93.39	0.93
	0	526.9	81.9	110.9	5.4966	-	-
	1x10^{-5}	514.0	63.5	88.4	2.6785	49.75	0.49
	5x 10^{-5}	511.1	74.5	106.8	2.5087	54.35	0.54
	1x10^{-4}	505.0	79.3	97.1	0.8741	84.09	0.84
35	5x10^{-4}	464.1	115.1	87.4	0.4707	91.43	0.91
	1x10^{-3}	472.8	80.7	70.6	0.4104	92.53	0.92
	0	528.3	88.5	110.5	10.9604	-	-
	1x10^{-5}	530.1	76.2	97.1	5.0565	53.86	0.53
	5x 10^{-5}	541.1	66.4	83.7	3.2026	70.78	0.70
45	1x10^{-4}	551.9	88.1	111.8	2.3515	78.54	0.78
	5x10^{-4}	555.9	82.9	100.1	1.7194	84.31	0.84
	1x10^{-3}	524.9	72.2	79.9	1.0379	90.53	0.90
	0	525.5	90.9	122.1	13.7492	-	-
	1x10^{-5}	556.0	68.4	117.2	6.0132	56.26	0.56
	5x 10^{-5}	551.9	76.1	89.5	5.3998	60.72	0.60
55	1x10^{-4}	527.1	78.8	109.7	5.1207	62.75	0.62
	5x10^{-4}	552.9	98.7	106.0	3.0648	77.70	0.77
	1x10^{-3}	550.1	92.0	112.4	3.0582	77.75	0.77

Table 6. Influence of temperature on electrochemical parameters of mild steel electrode immersed in 1 M HCl at different concentrations of **Ald** .

T (°C)	C (M)	$-E_{corr}$ (mV/SCE)	$-B_c$ (mV/dec)	B_a (mV/dec)	i_{corr} (mA cm^{-2})	EI_p (%)	θ
	0	471.7	77.3	98.5	1.2262	-	-
	$1x10^{-5}$	491.9	98.2	73.0	0.1750	85.72	0.85
	$5x10^{-5}$	489.3	120.4	71.1	0.1577	87.13	0.87
	$1x10^{-4}$	489.8	109.0	68.2	0.1312	89.30	0.89
25	$5x10^{-4}$	524.9	86.0	81.2	0.1032	91.58	0.91
	$1x10^{-3}$	467.8	129.8	71.8	0.0997	91.86	0.91
	0	526.9	81.9	110.9	5.4966	-	-
	$1x10^{-5}$	523.9	67.1	85.4	3.9074	28.91	0.28
	$5x\ 10^{-5}$	526.9	80.8	117.4	3.7399	31.95	0.31
	$1x10^{-4}$	531.5	74.0	96.1	2.7297	50.33	0.50
35	$5x10^{-4}$	534.3	69.3	91.8	2.4159	56.04	0.56
	$1x10^{-3}$	540.6	88.7	116.0	0.6430	88.30	0.88
	0	528.3	88.5	110.5	10.9604	-	-
	$1x10^{-5}$	531.7	77.3	96.0	5.0606	53.82	0.53
	$5x\ 10^{-5}$	502.9	75.3	110.6	4.1556	62.08	0.62
45	$1x10^{-4}$	509.1	64.9	93.5	3.1721	71.05	0.71
	$5x10^{-4}$	511.9	60.2	77.5	1.9917	81.82	0.81
	$1x10^{-3}$	522.2	73.8	112.5	1.9584	82.13	0.82
	0	525.5	90.9	122.1	13.7492	-	-
	$1x10^{-5}$	524.2	71.4	86.4	11.2575	18.12	0.18
	$5x\ 10^{-5}$	525.3	68.7	82.6	10.0515	26.89	0.26
55	$1x10^{-4}$	525.3	68.2	83.9	9.8894	28.07	0.28
	$5x10^{-4}$	527.1	81.5	136.1	4.7552	65.41	0.65
	$1x10^{-3}$	526.1	79.9	130.4	4.4679	67.50	0.67

4.4. Adsorption isotherm and thermodynamic parameters

The efficiency of organic compounds as a corrosion inhibitor mainly depends on its adsorption ability at the metal/solution interface. Therefore, it is essential to know the mode of adsorption and the adsorption isotherm that can give valuable information about the interaction of inhibitor and metal surface. The values of surface coverage (θ) calculated for different concentrations of inhibitors were used to test graphically to various adsorption isotherms including Freundlich, Langmuir, Temkin and Frumkin isotherms.

The observed inhibitive action L-S could be due to the adsorption of its molecules on the steel surface making a barrier for charge and mass transfer between the metal and the environment. It was found, at all studied temperatures (25C°–55C°) (table 7), the concentration of inhibitor increased by the fraction of steel surface covered by the adsorbed molecules (θ) increases.

Table 7. Thermodynamic parameters of adsorption for carbon steel in 1M HCl at different temperatures from Langmuir adsorption isotherm

Inhibitor	T (°C)	$K_{ads} \times 10^4$ (M^{-1})	$-\Delta G^0_{ads}$ (KJ mol^{-1})	$-\Delta H^0_{ads}$ (KJ mol^{-1})	ΔS^0_{ads} ($Jmol^{-1}$ K^{-1})
L	25	30.56	41.24	40.91	-3.26
	35	5.03	38.00		
	45	5.54	39.50		
	55	5.74	40.83		
Ald	25	55.56	42.73	87.57	-158.49
	35	0.92	33.64		
	45	6.44	39.03		
	55	0.83	35.58		

To see which kind of of adsorption isotherm our system obey, a graphic relation between the inhibitor concentration C_{inh} and C_{inh}/θ at different temperatures was drawn (Fig.6). Straight line with almost unit slope and correlation coefficient were obtained indicating that the system follows Langmuir adsorption isotherm. This indicates also, that mono-layer of adsorbed on the steel surface without interaction between the adsorbed molecules.

$$\frac{C_{inh}}{\theta} = \frac{1}{K_{ads}} + C_{inh} \quad \text{.....(12)}$$

where, K_{ads}s is adsorption constant. The K_{ads} values can be calculated from the intercept lines on the C_{inh}/θ axis. This is related to the standard free energy of adsorption (ΔG^0_{ads}) by

$$\Delta G^0_{ads} = -RT \ln(55.5 K_{ads}) \quad \text{.....(13)}$$

where 55.5 is the water concentration of the solution mL/S.

The negative values of ΔG^0_{ads} suggest that the adsorption of L and Ald molecule onto the steel surface is a spontaneous process and the adsorbed layer is stable. Usually the adsorption free energy involved in a chemisorption process is more negative by 25 kJ/mol [45]. We evaluated the values of $\Delta H_{ads}°$ and $\Delta S_{ads}°$ from the slop and intercept of the plot of ln K_{ads} versus 1/T (fig 7). Also the negative values of $\Delta H_{ads}°$ show that the adsorption is exothermal with an ordered phenomenon described by the negative values of $\Delta S_{ads}°$ [46].

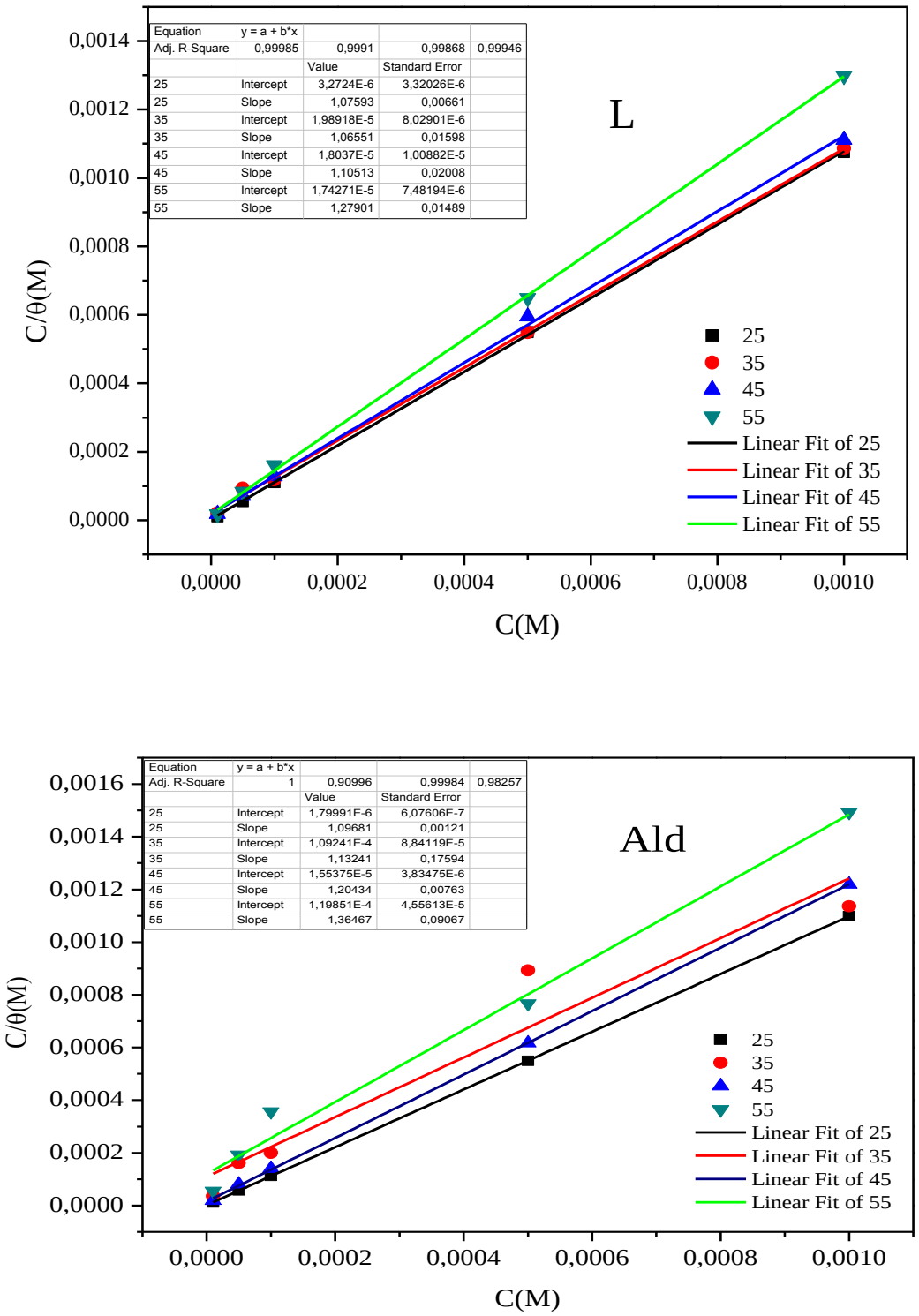

Equation	y = a + b*x			
Adj. R-Square	0,99985	0,9991	0,99868	0,99946
		Value	Standard Error	
25	Intercept	3,2724E-6	3,32026E-6	
25	Slope	1,07593	0,00661	
35	Intercept	1,98918E-5	8,02901E-6	
35	Slope	1,06551	0,01598	
45	Intercept	1,8037E-5	1,00882E-5	
45	Slope	1,10513	0,02008	
55	Intercept	1,74271E-5	7,48194E-6	
55	Slope	1,27901	0,01489	

Equation	y = a + b*x			
Adj. R-Square	1	0,90996	0,99984	0,98257
		Value	Standard Error	
25	Intercept	1,79991E-6	6,07606E-7	
25	Slope	1,09681	0,00121	
35	Intercept	1,09241E-4	8,84119E-5	
35	Slope	1,13241	0,17594	
45	Intercept	1,55375E-5	3,83475E-6	
45	Slope	1,20434	0,00763	
55	Intercept	1,19851E-4	4,55613E-5	
55	Slope	1,36467	0,09067	

Figure 6. Langmuir isotherm plots for carbon steel in 1 M HCl solution containing different concentration of **L** and **Ald** at different temperatures.

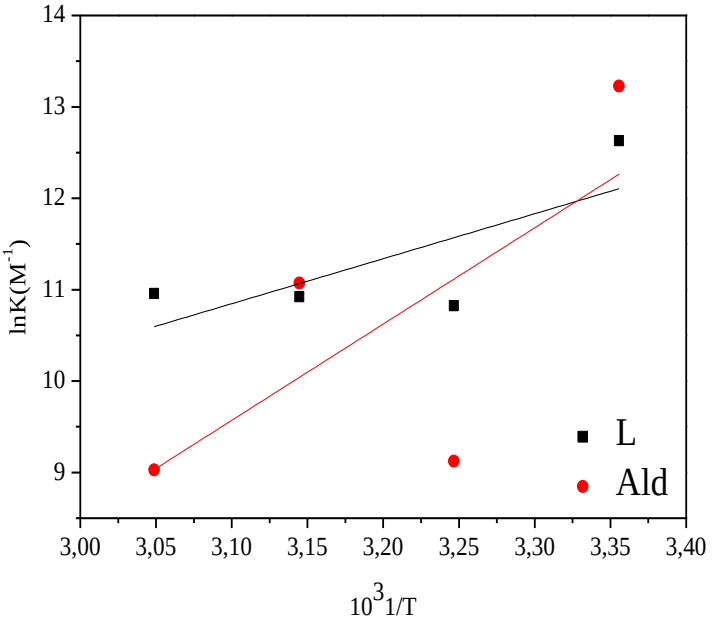

Figure 7. Plot of ln Kads versus 1/T of **L** and **Ald**

4.5. The potential of zero charge (PZC) and inhibition mechanism

Generally, the position of the corrosion potential (E_{corr}) with respect to the potential of zero charge (E_{PZC}) is used to determinate the surface charge of the metal fig 8.

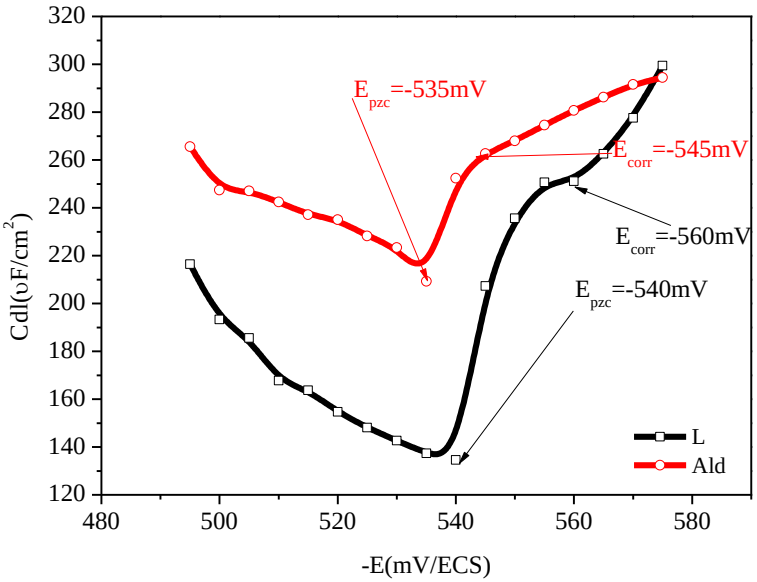

Figure 8. The plot of Cdl vs. applied potential for carbon steel in 1M HCl solution containing 10^{-3}M of inhibitors at 25°C

Mostly, the EIS is a useful method used in order to define the metal surface charge. The following equation can be used to calculate the net surface charge of the metal at the open circuit potential.

$$E_r = E_{corr} - E_{PZC} \quad \ldots\ldots\ldots\ldots\ldots\ldots\ldots\ldots\ldots\ldots\ldots\ldots(14)$$

where E_r is the Antropov's "rational" corrosion potential [47]. Table8 shows the values of E_{corr}, E_{PZC} (The potential of zero charge) and E_r for both inhibitors at 10^{-3}M concentration.

Table 8. Values of E_{corr} , E_{PZC} and E_r recorded for mild steel in 1 M HCl in presence of 10^{-3} M of **L** and **Ald** at 25 ℃.

Inhibitor	E_{corr} (mV/SCE)	E_{PZC} (mV/SCE)	E_r (mV/SCE)
L	-560	-540	20
Ald	-545	-535	10

In the inhibited solution the positive values of E_r means that in the presence of L and Ald in 1M HCl solution, the carbon steel surface carries the positive charge. Thus the Cl^- ions first adsorb onto the carbon steel surface which puts the carbon steel surface at negatively charged.

Moreover, the positive charge of the L and Ald forms an electrostatic bond with the Cl^- ions which are adsorbed on the surface of the carbon steel. Finally, a compressed layer of the adsorption molecules is formed. Furthermore, the inhibitory molecules can form acceptor-donor interactions between unshared electron pairs of N and O atoms and the unoccupied orbital of the iron atoms. The interaction between the C = N or C = O functional groups, the aromatic ring and the low-energy d orbitals of the surface iron atoms is responsible for chemical adsorption, because there is a physical adsorption between the positively charged protonated inhibitors and the Cl^- on the carbon steel surface by electrostatic interaction, so both types of adsorption (physisorption and chemisorption) can act on the surface of the positive- Steel [48].

4.6. Atomic force microscopy study

The Atomic force microscopy (AFM) has become a recent choice to study the surface morphology to nano and micro-level and is a powerful technique to investigate the effectiveness of the inhibitors against corrosion on the metal interface/solution [49]. The 2D and 3D images as well as the topography of the surface of the height profile are shown in Fig.9. These images show very rough surface of the carbon steel immersed in 1 M HCl and the reduction of the surface roughness in the presence of the **L** or **Ald**.

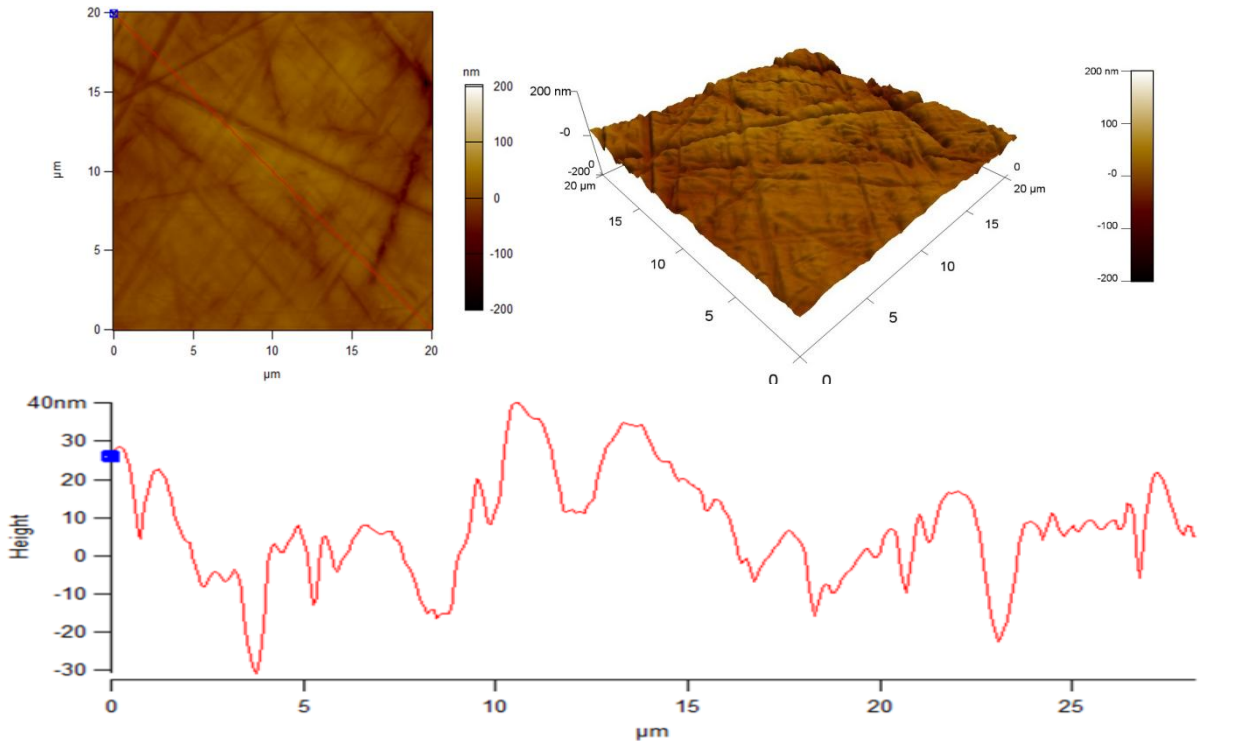

(a)

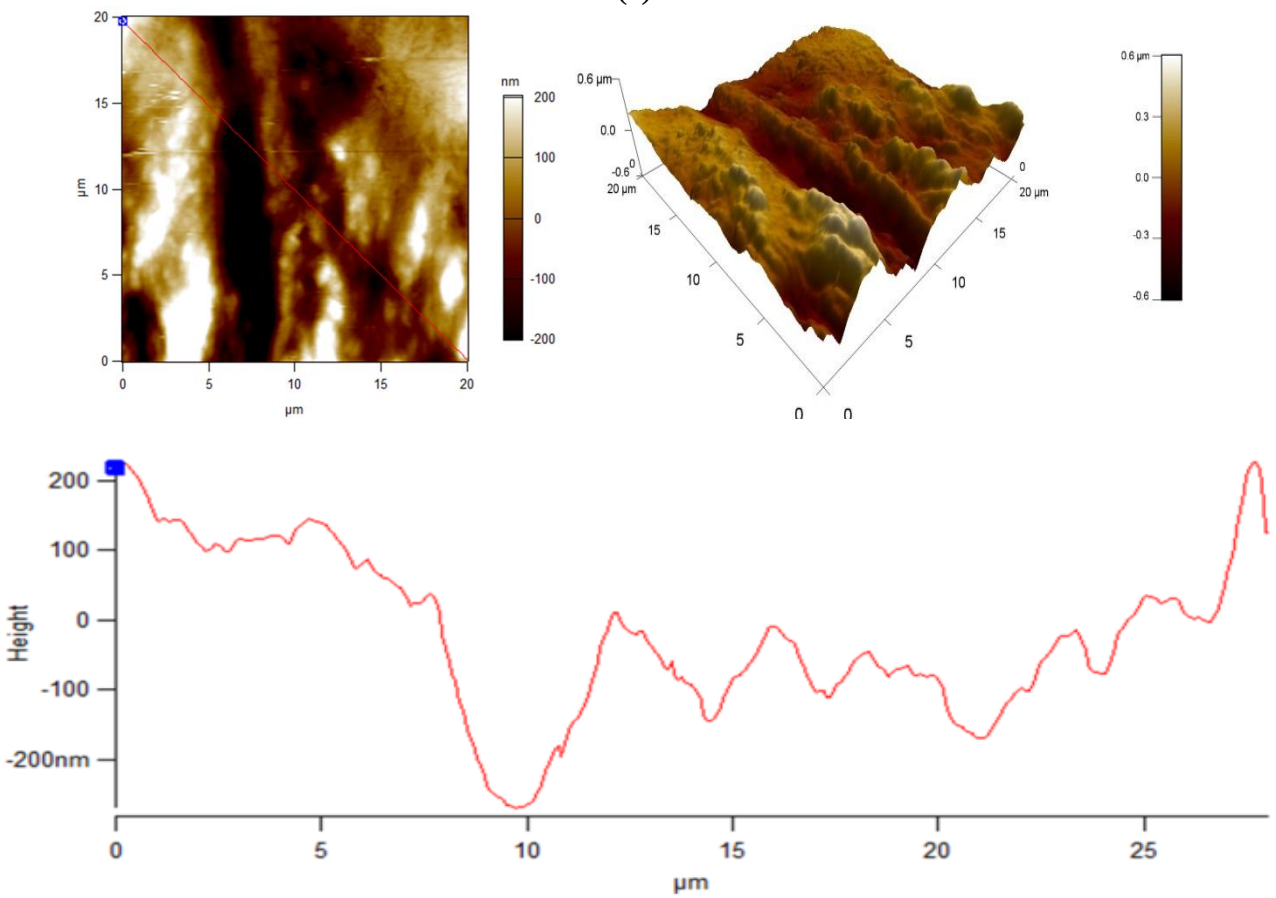

(b)

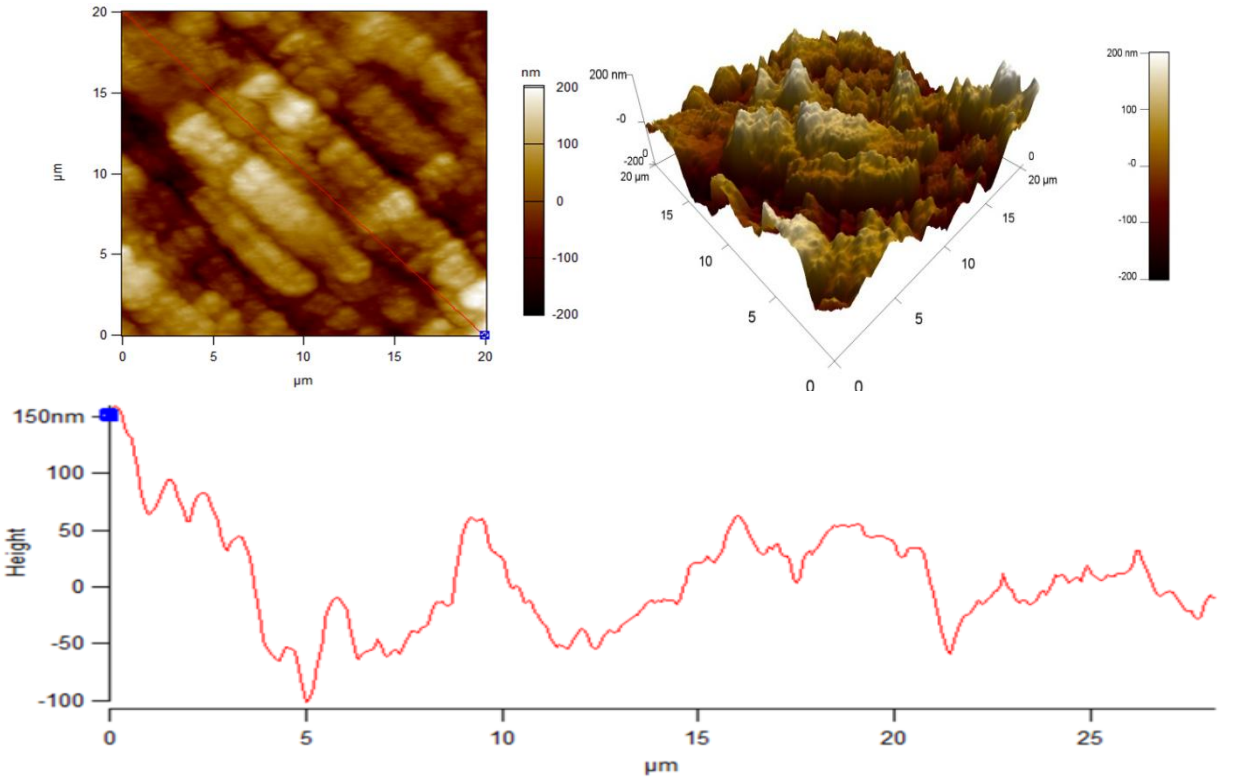

(c)

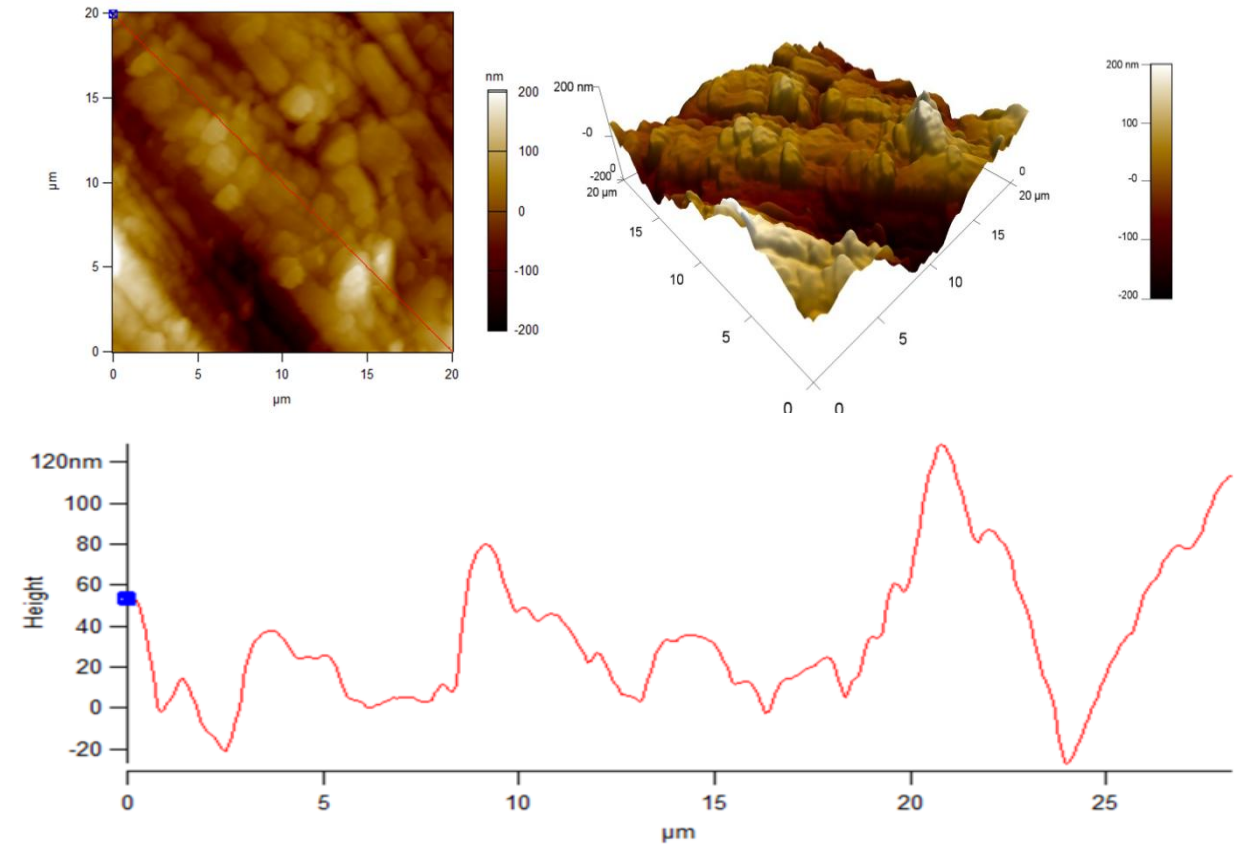

(d)

Figure 9. 2D, 3D and Height profile AFM images of carbon steel immersed in test solution for 24 h in the absence and presence of inhibitors (a) Polished Specimen (b) Uninhibited specimen in 1 M HCl (c) Inhibited specimen in 1 M HCl with **Ald** (d) Inhibited specimen in 1 M HCl with L.

To determine the Roughness Average, Roughness factor (*R*a) has been determined by the images. The Calculated values of *R*a has shown that the roughness of the surface of the metal immersed in 1 M HCl is past of 15.802 nm (*R*a of the polished metal surface) to 134.279 nm. However, as S decreased the *R*a is reduced to 62.761 Nm and 59.167 nm, which indicates that the development of the adsorbed layer of the inhibitor. These results are further supported by the size of the graphics profile [50]. The curve in the height of the sample has been polished for relatively stable with a slight fluctuation in 40 Nm as shown in Fig. 9. The most significant heterogeneity was observed for the specimen immersed in HCl 1 M without an inhibitor 200 nm, and it decreased in the presence of **Ald** and L the up to 150 nm and 120 nm respectively. These visual results confirm the results obtained by the other methods.

4.7. Quantum chemical calculations and molecular dynamic simulations

4.7.1. Quantum chemical calculations

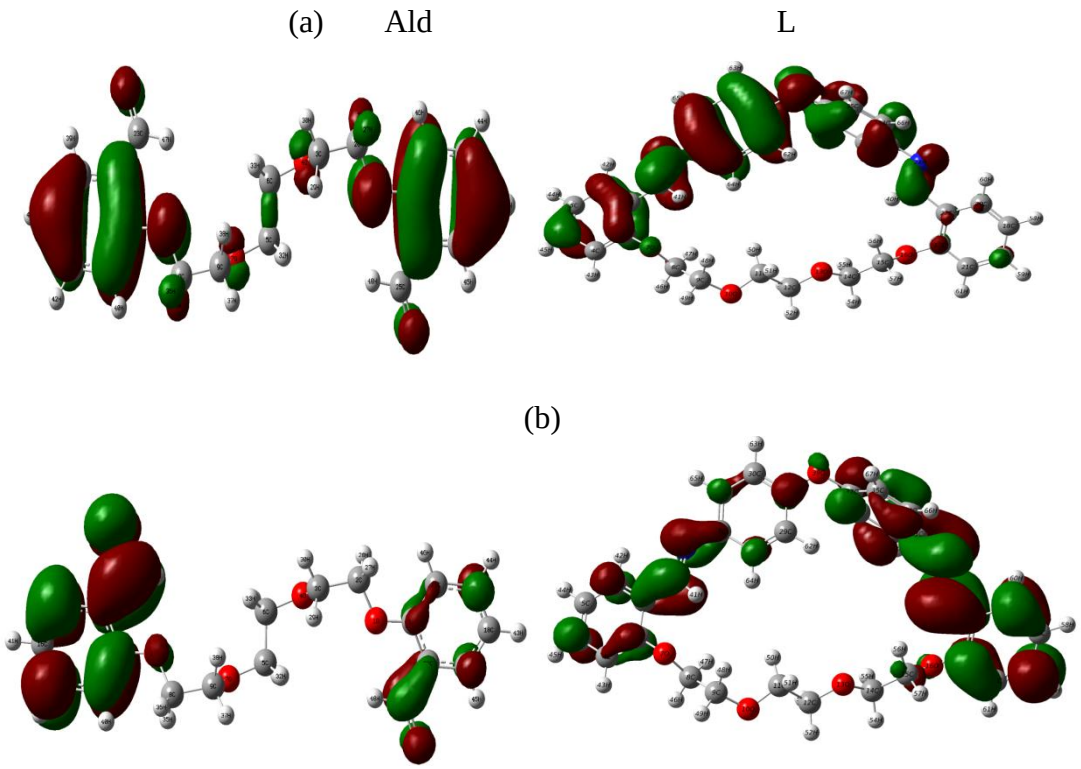

Figure 10. Frontier molecule orbital density distributions of the two molecules: HOMO (a) and LUMO (b).

From figure 10 it can be seen that HOMO and LUMO are distributed around heteroatoms and aromatic rings. The entire planar structure is the active center with several possible adsorbed sites for interaction. From the table 9, E_{HOMO} obeys the order: **L**> **Ald** which is the order of inhibition efficiency [51]. The low ΔE_{gap} values imply that the adsorption of the molecule on the metal surface is very easy

[11, 52, 53]. However, **L** has a lower ΔE_{gap} (3.785 eV) than **Ald** (4.803 eV), indicating the high acceptability of electrons in the iron d-orbit and high stability of [Fe -L] complex [54].

The dipole moment is a measure of the polarity of the bonding of diatomic molecules, which is related to the distribution of electrons in a molecular structure [55,56]. In our work, the dipole moments of **L** and **Ald** are 3.585 and 3.882 Debye, respectively which is higher than the dipole moment H_2O (1.88 Debye). The high dipole moment value of these compounds probably indicates strong dipole-dipole interactions between them and the metal surface [57].

The fraction of transferred electrons (ΔN) from the inhibitor to the carbon steel surface is also calculated. The values (ΔN) are correlated with the inhibition efficiency resulting from the electron donation. According to Lukovits [58], if (ΔN) <3.6, the inhibitory efficiency is increased by increasing the ability inhibitor to give electrons to metal surface. In this study, the ability to donate electrons to the metal surface follows the order of **L** >**Ald** , which is in good agreement with the order of inhibition efficiency of this compounds.

Table 9. Quantum chemical parameters derived for **L** and **Ald** calculated with the DFT/B3LYP method with 6-31G(d,p) basis set in gas (G) phase.

parameters	E_{HOMO} (eV)	E_{LUMO} (eV)	ΔE (eV)	μ (Debye)	I (eV)	A (eV)	χ (eV)	γ (eV)	σ $(eV)^{-1}$	ΔN
L	-5.474	-1.689	3.785	3.585	5.474	1.689	3.581	1.892	0.528	0.903
Ald	-6.370	-1.567	4.803	3.882	6.37	1.567	3.968	2.401	0.416	0.631

Natural bond Orbital (NBO) analysis provides an effective method for studying intra- and inter-molecular binding and also provides a practical basis for studying charge transfer in Molecular systems [59]. In order to study the interactions between the **L** and **Ald** orbitals and the free orbits of Fe atoms, the NBO values are calculated and listed in Table 10. Nitrogen, oxygen and some carbon atoms and the benzene rings of **L** and **Ald** have the negative charges, which are the most favored sites for bonding to the surface of carbon steel by donating electrons.

Table 10. NBO charges of the various atoms present in **L** and **Ald.**

Ald				L			
Atom	NBO Charge	Atom	NBO Charge	Atom	NBO Charge	Atom	NBO Charge
O1	-0.530	H40	0.244	C1	-0.154	H40	0.185
C2	-0.133	H41	0.245	C2	0.313	H41	0.191
C3	-0.123	H42	0.243	C3	-0.176	H42	0.266
O4	-0.583	H43	0.245	C4	-0.287	H43	0.251
C5	-0.132	H44	0.243	C5	-0.249	H44	0.241
C6	-0.132	H45	0.260	C6	-0.215	H45	0.242
O7	-0.583	H46	0.244	O7	-0.530	H46	0.200
C8	-0.133	H47	0.164	C8	-0.108	H47	0.219
C9	-0.123	H48	0.164	C9	-0.101	H48	0.204
O10	-0.530			O10	-0.602	H49	0.205

C11	0.363	C11	-0.103	H50	0.207
C12	0.363	C12	-0.125	H51	0.203
C13	-0.210	O13	-0.570	H52	0.201
C14	-0.169	C14	-0.126	H53	0.208
C15	-0.326	C15	-0.102	H54	0.207
C16	-0.268	O16	-0.568	H55	0.203
C17	-0.192	C17	0.327	H56	0.214
C18	-0.268	C18	-0.247	H57	0.210
C19	-0.192	C19	-0.213	H58	0.242
C20	-0.169	C20	-0.194	H59	0.243
C21	-0.326	C21	-0.283	H60	0.258
C22	-0.210	C22	-0.135	H61	0.246
C23	0.384	C23	0.121	H62	0.203
O24	-0.541	N24	-0.443	H63	0.257
C25	0.384	C25	0.084	H64	0.239
O26	-0.541	N26	-0.459	H65	0.255
H27	0.220	C27	0.119	H66	0.252
H28	0.229	C28	0.296	H67	0.250
H29	0.209	C29	-0.221	H68	0.217
H30	0.212	C30	-0.276	H69	0.180
H31	0.235	C31	-0.221		
H32	0.198	C32	-0.211		
H33	0.198	C33	0.117		
H34	0.235	C34	-0.219		
H35	0.229	C35	-0.253		
H36	0.220	C36	-0.230		
H37	0.212	C37	0.300		
H38	0.209	C38	-0.251		
H39	0.260	O39	-0.507		

Ald L

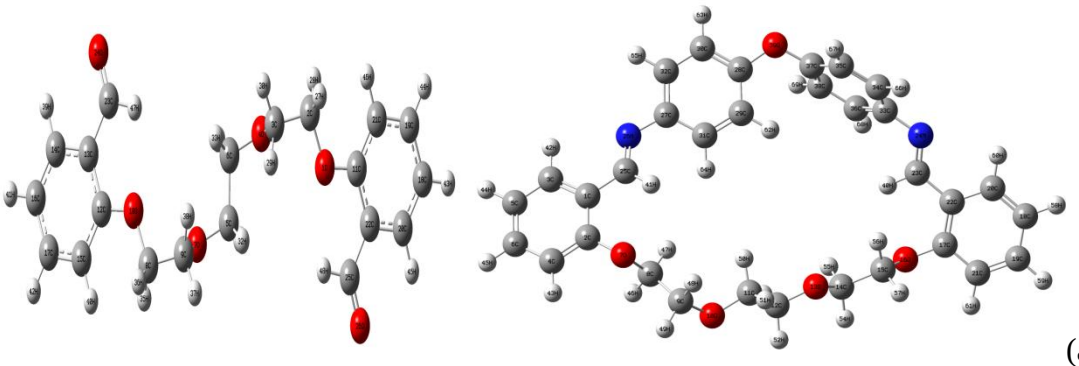

(a)

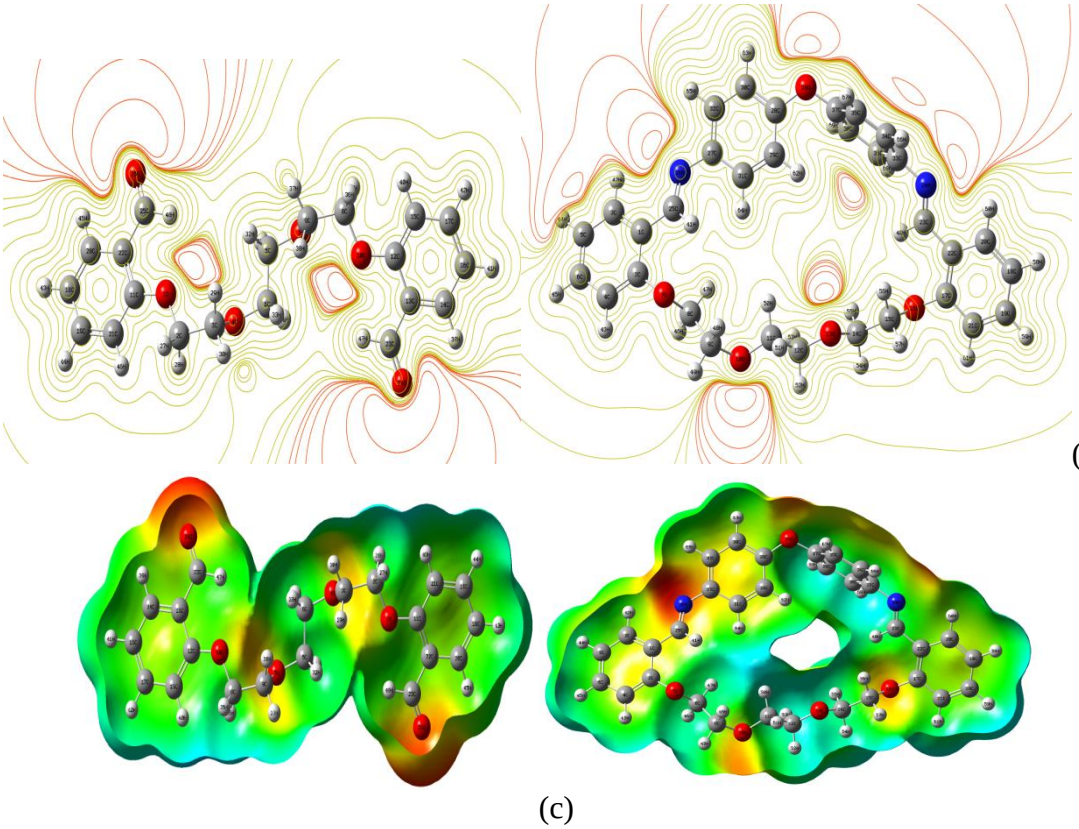

Figure 11. Quantum chemical results of Ald and L molecules calculated by the DFT/B3LYP method with 6-31G(d,p) basis set: (a) optimized molecular structure; (b) contour map of electrostatic potential with MBO charges values and (c) total electron density surface mapped with electrostatic potential

This can be seen from Fig. 11 that the **L** and **Ald** molecules have a general planar structure. This structural unit may be in favor of the larger contact surface if the molecule is adsorbed on the mild steel surface.

The molecular electrostatic potential (MEP) is related to electron density and is a very useful descriptor for understanding electrophilic etch sites and nucleophilic reactions [60]. The contour and the total electron density surface mapped with the molecular electrostatic potential (MEP) of **L** and **Ald** are shown in Fig.11, respectively. Negative (red1) regions of the MEP are related to nucleophilic reactivity and positive (blue) regions to electrophilic reactivity. As can be seen in this figure, it is clear that more electron-rich regions are mainly located around heteroatoms and conjugated double bonds. In this way, carbon steel acting as an electrophile is capable to attract the nucleophilic centers (heteroatoms with free electron pairs) of the inhibitory molecules [61].

4.7.2. Molecular dynamic simulations

Monte Carlo Simulations help to predict the interaction between the molecules of the inhibitor and metal surface. Fig12. Shows a typical plot of the distribution of energy (average total energy, Van

der Waals energy, electrostatic energy and intermolecular forces between **L** and **Ald** with the Fe (100) surface during the process of optimization.

Table 11. Outputs and descriptors calculated by the Monte Carlo simulation for adsorption of **L** and **Ald** on Fe(100)(Kcal/mol).

Inhibitor	Total energy	Adsorption energy	Rigid adsorption energy	Deformation energy	dEad/dNi
Ald	-141,641	-532,616	-187,617	-344,999	-532,616
L	-218,424	-224,674	-250,136	25,462	-224,674

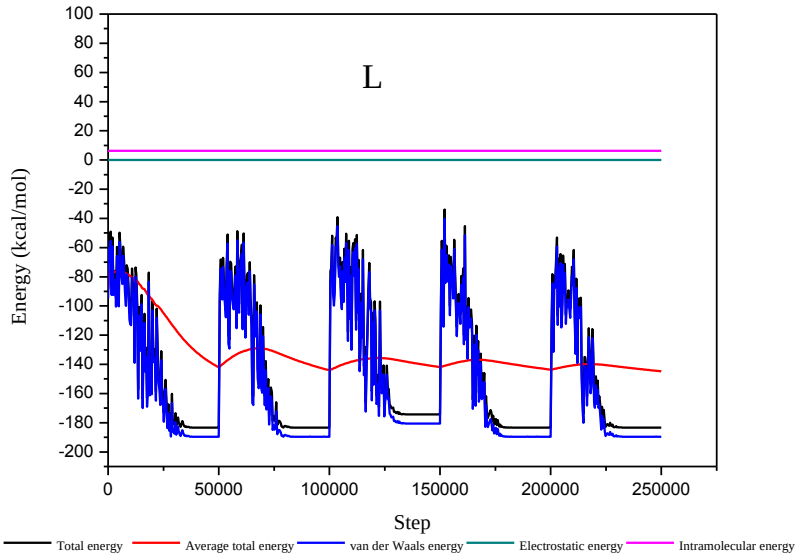

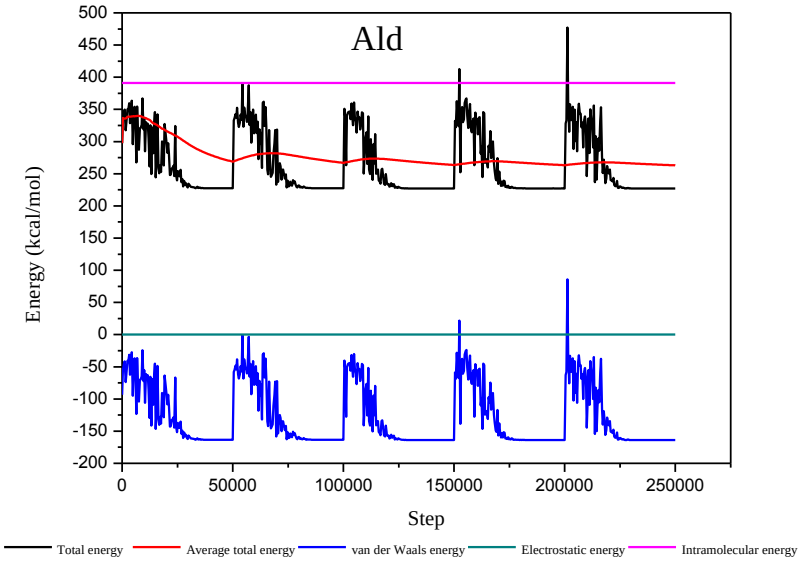

Figure 12. Typical energy profile for the adsorption of inhibitors on Fe (100) surface obtained using Monte Carlo simulations.

The more stable (low energy absorption of configurations of Ald, the on the Fe (100)) have been stimulated by the Monte Carlo simulation, and configurations are presented in Fig13.

Table11 shows the adsorption, rigid and deformation energies. The adsorption energy is due to the energy released during the course of the adsorbate adsorbed relaxd components on the substrate. The adsorption energy is the addition of adsorption and energies of rigid deformity of the adsorbate component. The high negative values of the energy of adsorption indicates a stronger interaction between a Fe(100) and an inhibitor molecule and it follows this order **L** > **Ald** which is in a good agreement with the experimental values of the effectiveness of the inhibition [62].

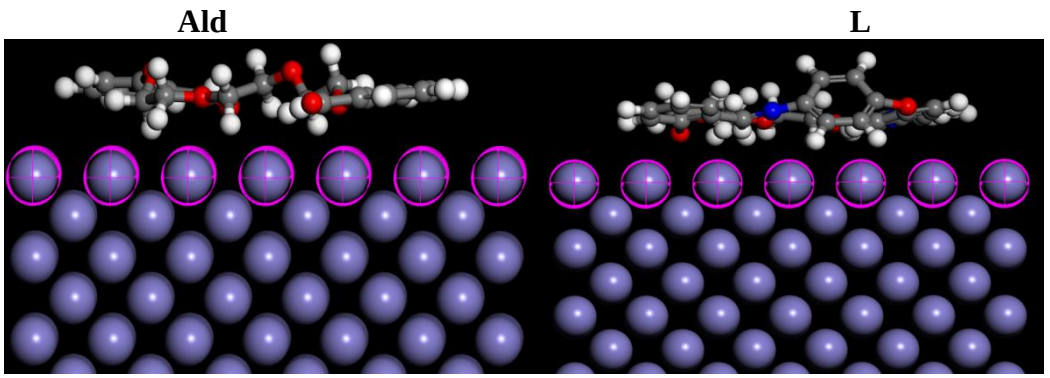

A

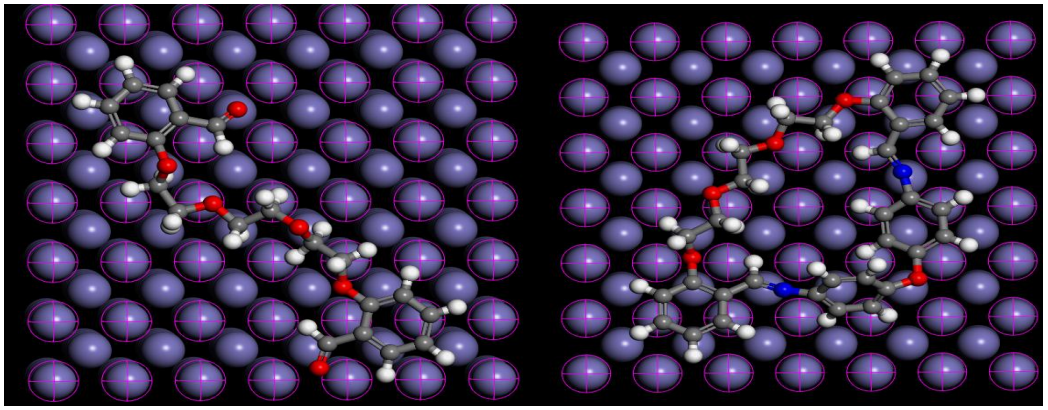

B

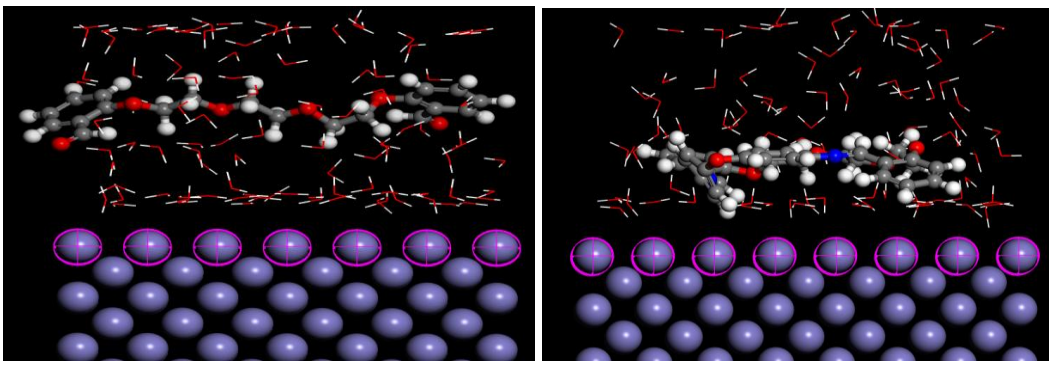

C

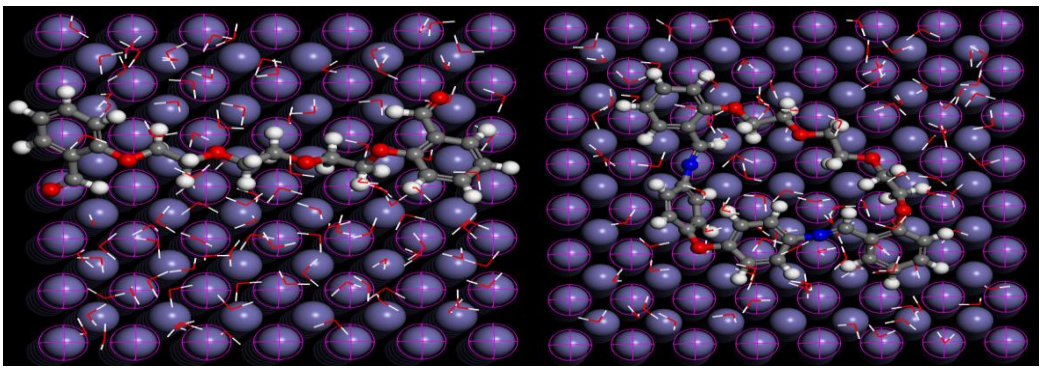

D

Figure 13. Equilibrium configurations of the adsorbed inhibitors molecules on Fe (100) surface in: (A) vacuum slabs (side view), (B) vacuum slabs (top view), (C) aqueous solutions (side view) and (D) aqueous solutions (top view).

5. CONCLUSION

The corrosion inhibition of compounds **L** and **Ald** for carbon steel XC48 in HCl was studied by theoretical and experimental (electrochemical) methods. The obtained results showed that:

1. The inhibition yield of these compounds increases with increasing inhibitor concentration

2. The adsorption of the molecules **L** and **Ald** obeys a Langmuir adsorption isotherm on the carbon steel Surface.

3. **L** is more stable and efficient than **Ald**.

4. The impedance diagrams obtained consist of a single capacitive loop which is generally interpreted as a charge transfer mechanism on a heterogeneous and irregular surface.

5. There is good agreement between the values of inhibitory efficiency determined by the three methods (gravimetry, polarization curves and electrochemical impedance spectroscopy).

6. The negative values of ΔG^0_{ads} and the high K_{ads} values indicate the spontaneity of the adsorption process and the stability of the adsorbed layer on the metal surface.

7. The values of ΔH_{ads} for inhibitors **L** and **Ald** are negative, indicating that these inhibitors are physisorbed and chemisorbed on the metal surface.

8. AFM study showed that the inhibitor (**L** and **Ald**) form a protective layer on the surface of the carbon steel.

9. **L** and **Ald** are excellent inhibitors for corrosion of carbon steel in 1 M and 2 M HCl, and behaves as mixed-type inhibitors.

10. The simulations of MD confirm that the molecules of **L** and **Ald** adsorb onto the Fe (100) surface in a virtually flat manner and that the values of the energies are in agreement with that of inhibition efficiency.

ACKNOWLEDGEMENT
This article was financially supported by Ferhat ABBAS University of Setif-1-Algeria.

References

1. P. Mourya, S. Banerjee, M.M. Singh, *Corros. Sci.*, 85 (2014) 352.
2. H. Hamani, T. Douadi, M. Al-Noaimi, S .Issaadi, D. Daoud, S. Chafaa, *Corros. Sci.*, 88 (2014) 234.
3. A. Rochdi, O .Kassou, N. Dkhireche, R. Touir, M .El Bakri, M .Ebn Touhami, M .Sfaira, B .Mernari, B. Hammouti, *Corros. Sci.*, 80 (2014) 442.
4. D. Daoud, T .Douadi, H. Hamani, S. Chafaa, M .Al-Noaimi , *Corros. Sci.*, 94 (2015) 21.
5. N. Chafai, S. Chafaa, K. Benbouguerra, D .Daoud, A .Hellal, M .Mehri , *J. Taiwan Inst. Chem. Eng.*, 70 (2017) 331.
6. G .Avci, *Mater. Chem. Phys.*, 112 (2008) 234.
7. I .B. Obot, N .O. Obi-Egbedi, *Corros. Sci.*, 52 (2010) 198.
8. I .Ahamad, R. Prasad, M. A. Quraishi, *Corros. Sci.*, 52 (2010) 3033.
9. E. S. Meresht, T .S. Farahani, J .Neshati, *Corros. Sci.*, 54 (2012) 36.
10. M .Gopiraman, N. Selvakumaran, D. Kesavan, R. Karvembu, *Prog. Org. Coat.*, 73 (2012) 104.
11. D .Daoud, T .Douadi, S .Issaadi, S .Chafaa, *Corros. Sci.*, 79 (2014) 50.
12. S .Issaadi, T. Douadi, A. Zouaoui, S .Chafaa, M.A. Khan, G. Bouet, *Corros. Sci.*, 53 (2011) 1484.
13. A.M .Al-Sabagh, N.M. Nasser, A. A. Farag, M.A.Migahed, A.M.F. Eissa, T .Mahmoud, *Egypt. J. Pet.*, 22 (2013) 101.
14. S.M. Abd El Haleem, S. Abd El Wanees, E.E. Abd El Aal, A. Farouk, *Corros. Sci.*, 68 (2013) 1.
15. A. Doner, E.A. Sahin, G. Kardas, O. Serindag, *Corros. Sci.*, 66 (2013) 278.
16. S. Kharchouf, L. Majidi, M. Bouklah, B. Hammouti, A. Bouyanzer, A. Aouniti, *Arab. J. Chem.*, 7 (2014) 680.
17. S. Kedy, N. Almhna , F. Kandil, *J. J. C*., 7 (2012) 73.
18. M. Frisch, G. Trucks, H. Schlegel, G. Scuseria, M. Robb, J. Cheeseman, G. Scalmani, V. Barone, B. Mennucci and G. Petersson, Gaussian 09, Revision A. 1, Gaussian Inc., Wallingford, CT. (2009)
19. R. Dennington, T. Keith and J. Millam, GaussView, Shawnee Mission, KS: Semichem, Incorporated Company Officers (2009).
20. A. D. Becke, *J .Chem. Phys.*, 98 (1993) 5648.
21. C. Lee, W. Yang, R. G. Parr, *Phys. Rev B.*, 37 (1988) 785.
22. W. Kohn, L.J. Sham, *Phys. Rev A.*, 137 (1965) 1697.
23. M. Arivazhagan, V.P. Subhasini, *Spectrochim. Acta. Part A.*, 91 (2012) 402.
24. M. S. Masoud, A.E. Ali, M.A. Shaker, G.S. Elasala, *Spectrochim. Acta .Part A.*, 90 (2012) 93.
25. V.S. Sastri, J.R. Perumareddi, *Corrosion-us.*, 53 (1997) 617.
26. Materials studio, 7.0 San Diego, CA: Accelrys Inc.; 2013.
27. ASTM, G 31–72, American Society for Testing and Materials, Philadelphia, PA,1990.
28. I.B. Obot, N.O. Obi-Egbedi, *Curr. Appl. Phys.*, 11 (2011) 382.
29. A. Döner, R. Solmaz, M. Özcan, G. Kardaş, *Corros. Sci.*, 53 (2011) 2902.
30. F. Bentiss, M. Lebrini, H. Vezin, F. Chai, M. Traisnel, M. Lagrenée, *Corros. Sci.*, 51 (2009) 2165.
31. X.H. Li, S.D. Deng, H. Fu, *J. Appl. Electrochem.*, 40 (2010) 1641.
32. F. Bentiss, M. Lebrini, M. Lagrenée, *Corros. Sci.*, 47 (2005) 2915.
33. M .A. Quraishi, Sudheer, E. Ebenso, *Int. J. Electrochem. Sci.*, 7 (2012) 9920.
34. X. Li, S. Deng, X. Xie, *Corros. Sci.*, 81 (2014) 162.
35. T. Ghailane, R. A. Balkhmima, R. Ghailane, A. Souizi, R. Touir, M. Ebn Touhami, K. Marakchi, N .Komiha, *Corros. Sci.*, 76 (2013) 317.
36. M.A. Hegazy, *Corros. Sci.*, 51 (2009) 2610.
37. B. Xu, W. Yang, Y. Liu, X. Yin, W. Gong, Y. Chen, *Corros. Sci.*, 78 (2014) 260.
38. J. Wang, C.N. Cao, J.J. Chen, M.D. Zhang, G.D. Ye, H.C. Lin, *J. Chin. Soc. Corros. Prot.*, 15 (1995) 241.
39. Q. Qu, Z.Z. Hao, L. Li, W. Bai, Y.J. Liu, Z.T. Ding, *Corros. Sci.*, 51 (2009) 569.

40. R. Solmaz, *Corros. Sci.*, 79 (2014) 169.
41. R. Solmaz, *Corros. Sci.*, 81 (2014) 75.
42. X. Li, X. Xie, S. Deng, G. Du, *Corros. Sci.*, 87 (2014) 27.
43. N. El Hamdani, R. Fdil, M. Tourabi, C. Jama, F. Bentiss, *Appl. Surf. Sci.*, 357 (2015) 1294.
44. H.H. Hassan, E. Abdelghani, M.A. Amin, *Electrochim. Acta.*, 52 (2007) 6359.
45. T. Tuken, N. Kıcır, N.T. Elalan, G. Sıgırcık, M. Erbil, *Appl. Surf. Sci.*, 258 (2012) 6793.
46. S. Issaadi, T. Douadi, S. Chafaa, *Appl. Surf. Sci.*, 316 (2014) 582.
47. B. El Mehdi, B. Mernari, M. Traisnel, F. Bentiss, M. Lagrenee, *Mater. Chem. Phys.*, 77 (2002) 489.
48. M. Yadav, L. Gope, N. Kumari, P. Yadav, *J. Mol. Liq.*, 216 (2016) 78.
49. B. Zhang, C. He, X. Chen, Z. Tian, F. Li, *Corros. Sci.*, 90 (2015) 585.
50. M. Mobin, M. Rizvi, *Carbohyd. Polym.*,156 (2017) 202.
51. F. Zhang, Y. Tang, Z. Cao, W. Jing, Z. Wu, Y. Chen, *Corros. Sci.*, 61 (2012) 1.
52. A. Rochdi, O. Kassou, N. Dkhireche, R. Touir, M. El Bakri, M. Ebn Touhami, M. Sfaira, B. Mernari, B. Hammouti, *Corros. Sci.*, 80 (2014) 442.
53. T. Ghailane, R.A. Balkhmima, R. Ghailane, A. Souizi, R. Touir, M. Ebn Touhami, K. Marakchi, N. Komiha, *Corros. Sci.*, 76 (2013) 317.
54. L. Li, X. Zhang, J. Lei, J. He, S. Zhang, F. Pan, *Corros. Sci.*, 63 (2012) 82.
55. N.O. Eddy, B.I. Ita, *J. Mol. Model.*, 17 (2011) 359.
56. E.S.H. El Ashry, A. El Nemr, S.A. Esawy, S. Ragab, *Electrochim. Acta.*, 51 (2006) 3957.
57. M.A. Hegazy, *Corros. Sci.*, 51 (2009) 2610.
58. I. Lukovits, E. Kalman, Zucchi, *Corrosion-us.*, 57 (2001) 3.
59. M. Snehalatha, C. Ravikumar, I. Hubert Joe, N. Sekar, V.S. Jayakumar, *Spectrochim. Acta A.*, 72 (2009) 654.
60. N. Okulik, A.H. Jubert, *Internet Electron. J. Mol. Des*., 4 (2005) 17.
61. H. Tian, W. Li, K. Cao, B. Hou, *Corros. Sci.*, 73 (2013) 281.
62. K.F. Khaled, *Appl. Surf. Sci.*, 256 (2010) 6753.